Thermal conductivity and thermal boundary resistance of amorphous Al 2 O 3 thin films on germanium and sapphire

Jessy Paterson, Dhruv Singhal, Dimitri Tainoff, Jacques Richard, Olivier Bourgeois

▶ **To cite this version:**

Jessy Paterson, Dhruv Singhal, Dimitri Tainoff, Jacques Richard, Olivier Bourgeois. Thermal conductivity and thermal boundary resistance of amorphous Al 2 O 3 thin films on germanium and sapphire. Journal of Applied Physics, 2020, 127 (24), pp.245105. 10.1063/5.0004576 . hal-02966841

HAL Id: hal-02966841
https://hal.science/hal-02966841

Submitted on 11 Aug 2023

HAL is a multi-disciplinary open access archive for the deposit and dissemination of scientific research documents, whether they are published or not. The documents may come from teaching and research institutions in France or abroad, or from public or private research centers.

L'archive ouverte pluridisciplinaire **HAL**, est destinée au dépôt et à la diffusion de documents scientifiques de niveau recherche, publiés ou non, émanant des établissements d'enseignement et de recherche français ou étrangers, des laboratoires publics ou privés.

Journal of Applied Physics ARTICLE scitation.org/journal/jap

Thermal conductivity and thermal boundary resistance of amorphous Al_2O_3 thin films on germanium and sapphire

Cite as: J. Appl. Phys. **127**, 245105 (2020); doi: 10.1063/5.0004576
Submitted: 20 February 2020 · Accepted: 9 June 2020 ·
Published Online: 23 June 2020

View Online Export Citation CrossMark

Jessy Paterson,[a] Dhruv Singhal, Dimitri Tainoff, Jacques Richard, and Olivier Bourgeois[b]

AFFILIATIONS

Institut Néel, CNRS, Univ. Grenoble Alpes, 38000 Grenoble, France

[a]**Electronic mail:** jessy.paterson@neel.cnrs.fr
[b]**Author to whom correspondence should be addressed:** olivier.bourgeois@neel.cnrs.fr

ABSTRACT

Sub-nanometer thickness accuracy and excellent conformity make atomic layer deposited films prevalent in modern electronics, continuously shrinking in size. The thermal resistance of these films plays a major role in the overall energy efficiency of miniaturized devices. We report very sensitive thermal conductivity measurements of amorphous Al_2O_3 thin films grown using atomic layer deposition in the temperature range of 100–300 K. The 3ω method is used to characterize these films ranging from 17.0 to 119.4 nm in thickness, using a series-resistor model to deconvolve the intrinsic thermal conductivity of the film from thermal boundary resistances inherently present in the multilayer system. The thermal conductivity of amorphous alumina films with a density of $2.77 \pm 0.14\,\mathrm{g\,cm^{-3}}$ is measured to be $1.73 \pm 0.08\,\mathrm{W\,m^{-1}\,K^{-1}}$ at 300 K. Measurements were carried out on germanium and sapphire substrates, leading to no substrate dependence of the films' thermal conductivity, within experimental accuracy. On the other hand, thermal boundary resistances of the systems Pt/Al_2O_3/substrate are observed to be strongly substrate-dependent, with values ranging from $2.1 \times 10^{-8}\,\mathrm{m^2\,K\,W^{-1}}$ to $3.7 \times 10^{-8}\,\mathrm{m^2\,K\,W^{-1}}$ at 300 K for films deposited on sapphire and germanium, respectively. These results provide further insights into the significance of interfaces in thermal transport across layered materials, in particular, for potential germanium-based devices.

Published under license by AIP Publishing. https://doi.org/10.1063/5.0004576

11 August 2023 09:03:29

I. INTRODUCTION

One of today's microelectronic industries foremost goals is a cumulative increase in power density, often reached by decreasing chip components down to nanometer sizes. This led to a soaring number of low-dimensional materials in current electronic devices accompanied with new challenges in the field of energy management. Low-dimensional materials such as thin films can be used for efficient thermal management, electrical insulation, or for their optical properties useful in the photovoltaic industry. Atomic Layer Deposition (ALD)-grown metal-oxide thin films such as Al_2O_3 have a wide range of applications, from the dielectric coating layer in transistor technology[1] to the assisting layer in lithography processing.[2,3]

The diversity of applications comes from their low temperature deposition, conformal coating, large breakdown electric field, and sub-nanometer level thickness accuracy.[4,5] Incorporation of high-k dielectric films to replace silicon dioxide in metal-oxide–semiconductor structures gave further relevance to ALD-oxide films in the last decade, while, in addition, the scope of research has been widened for non-silicon based devices in order to further improve devices performances. This consequently led to studies of a variety of stacked systems, among which Ge/ALD-Al_2O_3 structures were investigated because of the intrinsically high charge carrier mobility of germanium.[6–8] Ge/Al_2O_3 interfaces, which did not draw great attention in terms of thermal characterization, are highly relevant in the context of the Ge nanowire (NW) growth using techniques such as the Au-assisted vapor liquid solid process[9] or the template-assisted NW growth using nanoporous alumina.[10] Furthermore, ALD-Al_2O_3 thin films are often employed as insulating layers to prevent electrical leakage in electro-thermal measurements.[11,12] Consequently, accurate characterization of ALD-Al_2O_3 thin films' thermal conductivity and thermal interfacial resistances are compulsory for the efficient design of novel multilayered structures and for data extraction in thermal measurements involving ALD-Al_2O_3 thin films.

Published under license by AIP Publishing.

The development of accurate thermal characterization methods for low-dimensional materials still remains an active, stimulating scientific field. However, creating both a heat source and thermometer in size-constrained materials is challenging from a technological point of view—though this becomes possible due to ceaseless development of clean room fabrication methods. The interpretation of experimental data becomes more complex when the size of the probed material is commensurate to that of the heat source, thermometer, or to characteristic lengths of the heat carriers. Yet, this complexity can be used to probe intrinsic properties of heat carriers or non-Fourier heat conduction regimes such as phonon mean free path spectrum and ballistic heat conduction.[13–16]

In most cases, the thermal characterization of thin films is performed on a substrate, leading to an additional thermal interfacial resistance between the substrate and measured thin film. As the film thickness decreases, the contribution of the film thermal resistance becomes comparable to that of the interface, leading to a severe underestimation of the film thermal conductivity. The 3ω method[17] has proven effective in measuring thermal conductivity of thin films, substrates, and in estimating the interfacial thermal resistances [most commonly referred to as Thermal Boundary Resistance (TBR)] from the system substrate/film/heater.[10,18–22] In this regard, in this work, we present very sensitive thermal conductivity measurements of Al_2O_3 films of varying thicknesses (17–119 nm) grown by Atomic Layer Deposition on sapphire and germanium using the 3ω method. Temperature dependence of the thermal conductivity of Al_2O_3 thin films and substrates are presented along with the interpolated TBR of the substrate/Al_2O_3/Pt system. These results show the significant impact that Al_2O_3 thin films and TBRs may have on the global thermal balance of layered structures present in functioning devices, especially for systems containing Ge/ALD-Al_2O_3 interfaces.

II. METHODS

A. Sample preparation

Amorphous Al_2O_3 thin films were deposited on two different crystalline substrates (sapphire and germanium) by ALD using a Cambridge Nanotech Savannah S100 ALD system. Prior to deposition, each substrate was cleaned using acetone, rinsed using ethanol, and then submitted to a soft O_2 plasma for 100 s to remove any residual contamination that could alter the interface quality. Then, each sample was subjected to the same ALD deposition conditions: a four cycle process alternating between the flow of the precursor (trimethylaluminum, TMA) and H_2O, using N_2 as a purge gas. Growth temperature was stabilized to 150 °C and the number of cycles were 145, 350, 500, 750, and 1000, leading to the thicknesses of the Al_2O_3 thin films of 17.0, 41.0, 60.1, 89.7, and 119.4 nm, respectively. X-ray reflectivity (XRR) has been used to measure all the film thicknesses. Using Rutherford backscattering spectrometry (RBS) along with XRR, the density of the film was measured to be $2.77 \pm 0.14\ \mathrm{g\,cm^{-3}}$, in good agreement with other ALD-Al_2O_3 films grown at a similar temperature.[4]

The metallic heating element used for 3ω measurements has been fabricated using standard clean room techniques consisting of laser lithography patterning followed by platinum magnetron sputtering (100 ± 20 nm) and lift-off. It is about 5 μm wide and spans 500 μm between the two voltage leads; these dimensions have been measured using scanning electron microscopy for each sample. We note that no adhesion layer has been used prior to the metallic sputtering.

B. Thermal characterization

Thermal conductivity measurements of ALD-Al_2O_3 thin films were performed using the 3ω method. The 3ω method consists in measuring the thermal impedance created by a specimen of interest, when submitted to a heat flux. The heat flux is created by applying an alternative current of frequency ω through a metallic line deposited on top of the specimen. Joule heating occurring at 2ω leads to an oscillation of the metallic line resistance at the same frequency, hence producing a small 3ω voltage. The 3ω voltage, which is proportional to the temperature rise $\Delta T_{2\omega}$ sensed by the metallic line, is related to the thermophysical properties of the specimen. The metallic line acting both as a heater and a thermometer will be henceforth referred to as the transducer. After the transducer calibration and by means of a fitting procedure described subsequently, we extract the thermal conductivity of the film and substrate of interest along with the sum of TBRs.

1. Experimental setup for the 3ω measurement

The temperature oscillation amplitude of the transducer is measured using resistive thermometry through voltage measurements using the relation $\Delta T_{2\omega} = 2V_{3\omega}/I_{1\omega}(dR/dT)$, where V, R, and I represent voltage, transducer's resistance, and current, respectively.[17,23] Subscripts refer to frequency harmonics. The third harmonic voltage is always present alongside a large ohmic voltage background. Indeed, the voltage ratio $V_{1\omega}/V_{3\omega}$ scales as $(\beta\Delta T_{2\omega})^{-1}$, where β is the temperature coefficient of resistance (TCR) of the transducer, defined as $\beta = (1/R)(dR/dT)$. In this study, a platinum transducer was used for which the measured TCR is around $2 \times 10^{-3}\ \mathrm{K^{-1}}$ at room temperature, as presented in Fig. 1.

11 August 2023 09:03:29

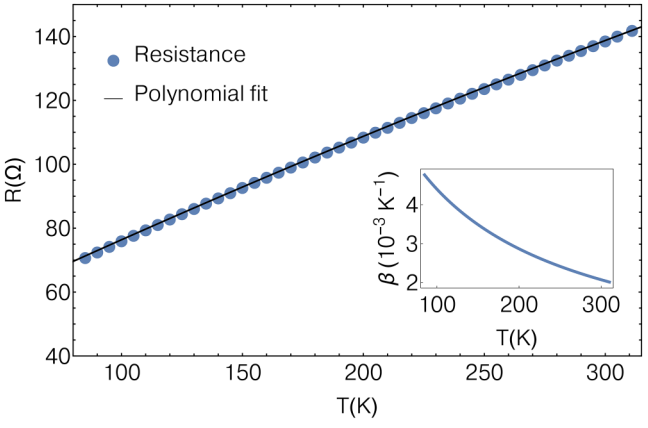

FIG. 1. Measured resistance vs temperature for a platinum transducer. Every transducer has been measured separately prior to 3ω measurements, only one is presented here for clarity. The black line represents the best fit to the data using a second order polynomial. In the inset is displayed the temperature coefficient of resistance derived from the best fit to the data.

Published under license by AIP Publishing.

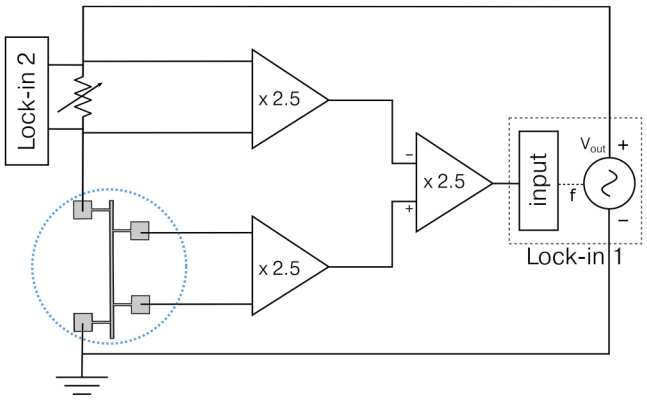

FIG. 2. Simplified schematic of the setup used for a 3ω experiment as described in the main text. Lock-in 1 output voltage is used to source the circuit and read the third harmonic of the voltage, while lock-in 2 reads the current from the known variable resistance. Part of the circuit (within the blue-dashed circle) is immersed inside a cryostat and put under vacuum ($\approx 10^{-5}$ mbar). The circuit is controlled from a computer so that the programmable resistance is automatically changed to match that of the transducer when the experiment is run as a function of temperature.

The measured $\Delta T_{2\omega}$, usually lying within the range of 0.1–2 K, leads to a ratio $V_{1\omega}/V_{3\omega}$ greater than 10^3. Consequently, in order to enhance the $V_{3\omega}$ reading sensitivity, we use a differential bridge presented in Fig. 2. We use lock-in 1 (AMETEK 7230) output voltage to source the circuit. A programmable resistance (IET PRS-B-7.001) is placed in series and set to match the transducer resistance. It is further used to read the circuit current using lock-in 2. The differential bridge is built from three INA103 instrumentation amplifiers, with the purpose of considerably lessening the ohmic 1ω voltage. In the first stage of the bridge, the same voltage drops across both the transducer and the programmable resistance, the latter assumed to have negligible temperature coefficient of resistance. Consequently, the output voltage in the second stage of the bridge contains the small $V_{3\omega}$ immune from the large ohmic background. Amplification has been chosen so as to increase the signal for easier detection while keeping it low enough for the second stage of the bridge not to overload. The resulting signal is read using lock-in 1 input.

2. Data reduction procedure

As in many frequency dependent thermal characterization techniques, the thermal penetration depth—the characteristic length over which the temperature amplitude decays toward zero—is closely related to the heat source excitation frequency, in this case, the electrical current frequency. Introducing the thermal wavevector q to be consistent with the literature notation,[17,24] the thermal penetration depth is defined as $|1/q| = \sqrt{\alpha/\omega_{\text{th}}}$, where $\alpha = k/\rho C_p$ is the thermal diffusivity of the material and ω_{th} is the thermal excitation frequency ($\omega_{\text{th}} = 2 \times \omega_e$). The experiment consists in heating the sample using the transducer and measuring the temperature response of this transducer as a function of its excitation frequency. Fitting the thermal response of the calibrated transducer using an adapted heat conduction model permits extraction of several thermal properties of the system under study.

Given the expected high thermal conductivity ratio between the thin film and its substrate (germanium or sapphire) in addition to the high contrast between the heater half-width (2.5 μm) and film thickness ($\approx$17–120 nm), a one-dimensional model is relevant to describe the thermal resistance of the film on top of its substrate.[25] The measured thermal conductivity of the films reported in this work are, therefore, cross-plane (parallel to the growth direction, y-axis in Fig. 3). After solving the heat equation with appropriate geometry and boundary conditions, the temperature oscillation at 2ω sensed by the transducer can be written as[25]

$$\Delta T_{2\omega} = \frac{p}{\pi l k_{s_y}} \int_0^\infty \frac{1}{\sqrt{k_{s_{xy}}\lambda^2 + \frac{i2\omega_e}{\alpha_s}} \tanh\left(\sqrt{k_{s_{xy}}\lambda^2 + \frac{i2\omega_e}{\alpha_s}} d_s\right)} \times \frac{\sin^2(b\lambda)}{(b\lambda)^2} d\lambda + \frac{p}{2bl} R_{\text{th}}, \tag{1a}$$

$$\alpha_s = \frac{k_{s_y}}{\rho_s C_{p_s}}, \tag{1b}$$

where p is the peak electrical power dissipated by the transducer of length l and half-width b and ω_e is the angular modulation of the electrical frequency. k_{s_y}, ρ_s, C_{p_s}, $k_{s_{xy}}$, and d_s stand for the substrate's cross-plane component of the thermal conductivity, density, heat capacity, thermal anisotropy, and thickness, respectively. The first part of the right hand side of Eq. (1a) reflects the substrate contribution to the measured thermal resistance, whereas the second part represents the film and interfaces contribution to the total thermal resistance. The hyperbolic tangent term comes from applying adiabatic conditions at the bottom of the substrate, representing a non-perfect interface between the substrate and sample holder. For the germanium substrate, we use $k_{s_{xy}} = k_{s_x}/k_{s_y} = 1$ for the fitting of Eq. (1), which we assume is a safe assumption given its crystal structure. For the sapphire substrate, it might not be the case and we use $k_{s_{xy}} = 1.1$. The error introduced from the substrate's thermal anisotropy is discussed in the Appendix and included in the uncertainty analysis described afterward.

In this study, we assume a simple 1D series-resistor model for the thermal resistance of the film and interfaces,[26] as depicted in Fig. 3. Thereby we write the thermal resistance R_{th} as

$$R_{\text{th}} = \frac{d_f}{k_f} = R_{\text{int}} + \frac{d_f}{k_i}, \tag{2}$$

where d_f refers to the film thickness, k_f its apparent thermal conductivity, R_{int} to the sum of TBRs (heater/film + film/substrate), and k_i stands for the intrinsic thermal conductivity of the film, i.e., independent of its thickness. The latter assumption is expected to hold true given the small mean free path of the heat carriers in amorphous solids ($\approx$1 nm)[27] in comparison to the films thicknesses (17−−119 nm) and have been experimentally verified[28,29] for ALD-Al_2O_3 films with smaller thicknesses than that used in the present work. The simple form of Eq. (2) also implicitly assumes a

11 August 2023 09:03:29

Published under license by AIP Publishing.

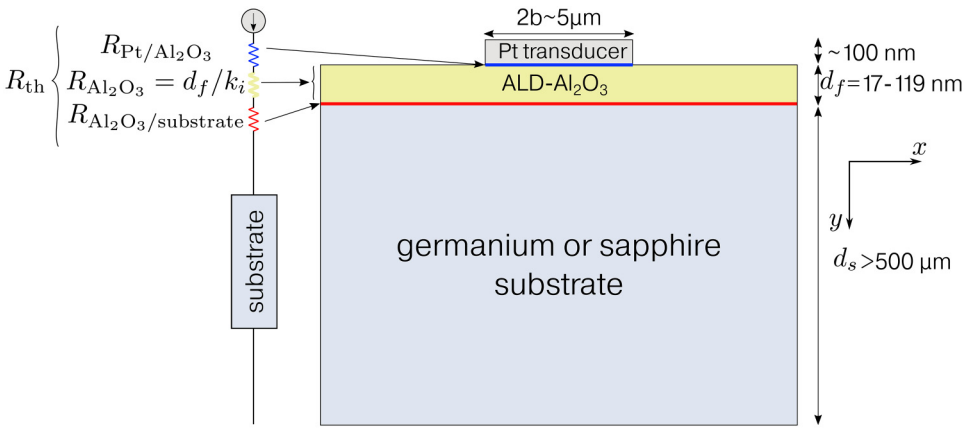

FIG. 3. Schematic representation of the system measured in this work, either on a sapphire or germanium substrate. On the left is displayed a simplified thermal circuit in term of thermal resistances in series with the heat source. The two TBRs, R_{Pt/Al_2O_3} and $R_{Al_2O_3/substrate}$, are highlighted in blue and red, respectively.

constant value of R_{int} among films of increasing thickness. XRR measurements of the alumina films indicate that their top surface rms roughness vary little as a function of the film thickness (<0.15 nm rms), consistent with other report quantifying the surface roughness of ALD-deposited films as a function of their thickness.[30] Furthermore, since our films are at least 17 nm thick, their stoichiometry is expected to be similar among all films,[8] and, therefore, we assume that R_{int} is constant for all samples (for a given substrate).[31]

Besides being relatively simple, Eq. (2) provides one significant benefit; the film heat capacity does not need to be known to extract its thermal conductivity. We can then calculate the sum of thermal boundary resistances, R_{int}, with the cost of performing multiple measurements using films of increasing thicknesses.

To summarize, for extracting the thermal conductivity of the film, substrate, and the sum of TBRs, we primarily fit the measured $\Delta T_{2\omega}$ to Eq. (1) to obtain k_s and R_{th} as shown in Fig. 4. The substrates heat capacity have been measured separately using a commercially available physical property measurement system from quantum design. We then fit each R_{th} for each thin film thickness according to Eq. (2). From the slope of Eq. (2), we extract the intrinsic thermal conductivity of the Al_2O_3 film. R_{int} is inferred from the intercept extrapolated to zero thickness.

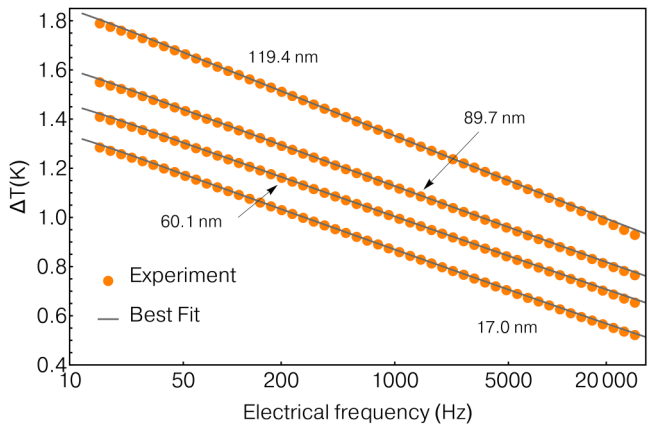

FIG. 4. Measured ΔT vs electrical frequency for four thicknesses of Al_2O_3 deposited on sapphire substrate at 300 K (41.0 nm not shown for clarity). Filled circles are data, and solid lines are the best fit to Eq. (1). Peak power dissipated lies between 11 and 12 mW for the four transducers.

C. Uncertainty analysis

To quantify the uncertainty of our results, we use a so-called "Monte Carlo" approach, an expedient way to quantify error propagation in nonlinear fitting.[32,33] First, using least square regression, we fit our measured dataset (frequency, $\Delta T_{2\omega}$) to Eq. (1) using our measured control variables (thermometer width and length, substrate heat capacity and density, power dissipated, substrate anisotropy) to numerically extract k_s and R_{th}. Next, we build a new synthetic dataset (frequency, ΔT_{synth}) from the previously extracted (k_s, R_{th}) values and perturbed control variables, the latter being obtained by randomly drawing a value from their normal distribution which has been either measured or represent our best guess. We then introduce the experimental error of the measured $\Delta T_{2\omega}$ in a similar manner, i.e., we randomly draw a sample value from its normal distribution. Each synthetic data set contains errors coming from the experimental accuracy of our measurement, along with the error coming from our controlled variables. Repeating these steps N times, we obtain N synthetics sets of data. Fitting each new (frequency, ΔT_{synth}) dataset using measured control variables gives a distribution of (k_s, R_{th}) from which we can extract relevant statistical parameters, such as confidence intervals. Eventually, we find the confidence intervals for R_{int} and $k_{Al_2O_3}$ fitting Eq. (2) using (film thickness, R_{th}) datasets, where the distribution of R_{th} has been constructed in the previous step.

We show in Fig. 5 the resulting histograms from the derived thermal conductivity of sapphire and germanium substrates on which Al_2O_3 thin films were grown, using $N = 1000$. Five different thicknesses of the films were measured, resulting in five different substrates (we could not reliably measure the 17 nm Al_2O_3 deposited on germanium, due to possible electrical leakage). This allows—in addition to the N Monte Carlo runs—to acquire another statistical indicator, illustrating the repeatability of the measurement. It is clear from Fig. 5 that the repeatability of the

11 August 2023 09:03:29

Published under license by AIP Publishing.

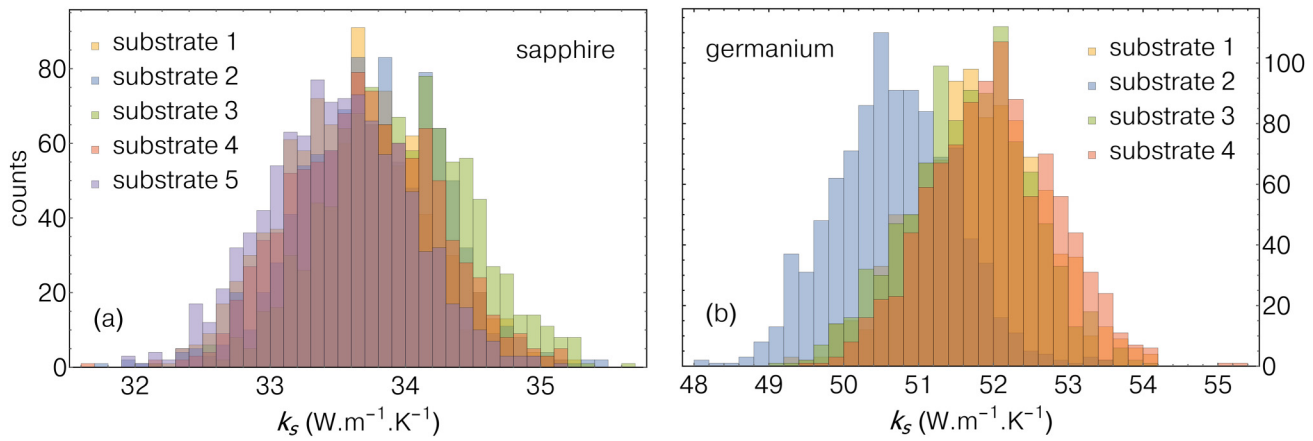

FIG. 5. Histograms of the thermal conductivity for (a) sapphire and (b) germanium substrates, derived from datasets including errors coming from input parameters and experimental uncertainty. Numbers 1–5 refer to substrates on which Al_2O_3 thin films were grown resulting in thicknesses ranging from 17.0 to 119.4 nm. These values were derived at 300 K, using $N = 1000$ random draws.

measurement is satisfying, since the five values of the derived sapphire thermal conductivity are within less than 2% of the calculated mean value of 34 W m^{-1} K^{-1} at 300 K, in good agreement with reported values.[34,35] For the germanium thermal conductivity, the four extracted values are consistent within 5% to the mean value of 52 W m^{-1} K^{-1} at 300 K, agreeing well with measured values for doped germanium.[36,37] The overlapping between distributions suggests that the measured small variations coming from the repeatability of the experiment corroborates well with the confidence intervals derived from inputs parameters and experimental uncertainty.

III. RESULTS AND DISCUSSION

To ascertain the validity of our measurement, we have carried out measurements using several currents and, hence, various dissipated power. The linearity between the $V_{3\omega}$ voltage and the current's third power ensures the thermal signature of the measured voltage (see Fig. 6), for several frequencies. The fitting of the temperature oscillation vs frequency is performed up to ≈30 kHz, as shown in Fig. 4. This allows us to disregard most of high frequency spurious effect coming from capacitive coupling or harmonic distortion present in the electrical circuit. Most importantly, the lower frequency used for the fitting is chosen such that the thermal penetration depth remains smaller than the substrate thickness at each temperature. The upper frequency is restricted by the one-dimensional model we chose to use: the thermal penetration depth should be much larger than the film thickness, which is readily attained given the small thickness of the films studied in this work.

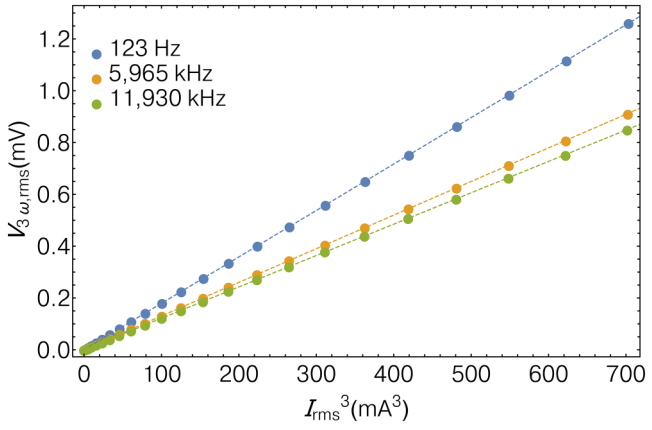

FIG. 6. Measured 3ω voltage as a function of the third power of the electrical current for several frequencies at 300 K. Dashed lines are linear fits to the data.

A. Intrinsic thermal conductivity of ALD-Al_2O_3 thin films

The measured thermal resistances as a function of film thickness are plotted in Fig. 7 for both substrates and several temperatures. From these plots, the intrinsic thermal conductivity of the films and the extrapolated TBR of the Pt/Al_2O_3/substrate system are extracted, as explained previously. The intrinsic thermal conductivity of the ALD-Al_2O_3 thin films is plotted vs temperature in Fig. 8. The values extracted from either substrate are consistent with each other, within the accuracy of the measurements, represented as tinted bands.

Tinted bands in Figs. 8 and 9 represent 68% confidence intervals (CIs) derived using the method detailed in Sec. II, representing values falling within one standard deviation of the mean for a normal distribution. No substrate dependence of the film thermal conductivity is observed in the temperature range explored, within our experimental accuracy, which is consistent with other reports.[21,29] The thermal conductivity of the amorphous Al_2O_3 films range from 0.80 W m^{-1} K^{-1} at 100 K to 1.73 W m^{-1} K^{-1} at 300 K (see Table I). The value at 300 K is as well in very good agreement with other values reported for Al_2O_3 films grown in similar conditions. Indeed, literature values lie between 1.3

11 August 2023 09:03:29

Published under license by AIP Publishing.

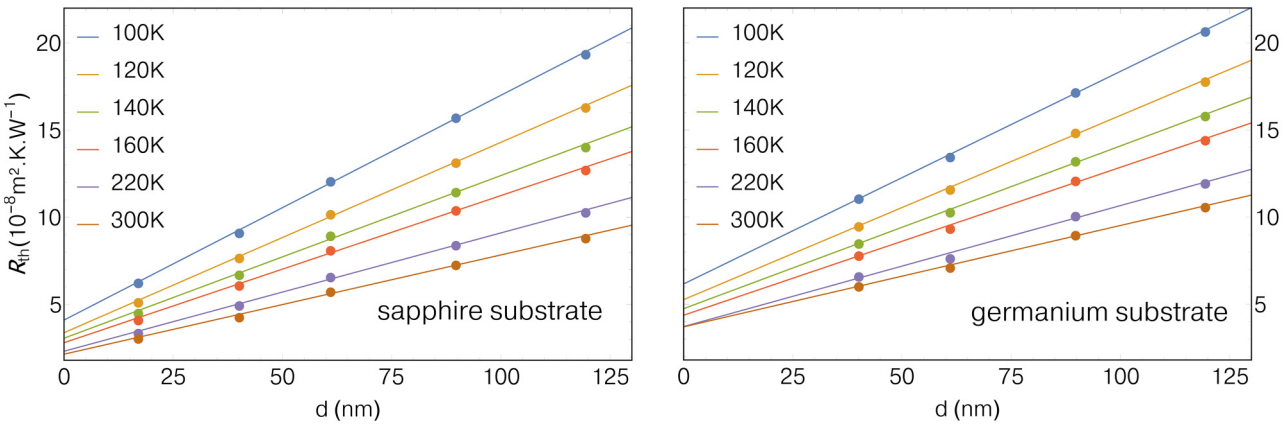

FIG. 7. Measured thermal resistances of the films as a function of their thickness, for several temperatures. Solid lines are linear fits to the data. Thermal boundary resistances are inferred from the intercepts of the fits extrapolated to zero thickness, whereas the intrinsic thermal conductivity of the films is derived from their slope.

and 2.4 $W\,m^{-1}\,K^{-1}$, depending on the growth technique and conditions.[21,28,38,40–44]

Since the thermal conductivity of amorphous ALD-Al_2O_3 is known to be significantly density dependent,[28] we compare the thermal conductivity of the present measurements to reported values of ALD-Al_2O_3 films with known density. For measured densities[45] of 2.72 $g\,cm^{-3}$ and 3.15 $g\,cm^{-3}$, DeCoster *et al.* reported, at room temperature, thermal conductivities of 1.35 $\pm$ 0.21 $W\,m^{-1}\,K^{-1}$ and 1.87 $\pm$ 0.26 $W\,m^{-1}\,K^{-1}$, respectively, using time-domain thermoreflectance (TDTR).[29] Lee *et al.* reported 1.99 $\pm$ 0.16 $W\,m^{-1}\,K^{-1}$ for films with a density of 3.3 $\pm$ 0.1 $g\,cm^{-3}$ using a similar 3ω method.[21] Scott *et al.*[38] reported 1.50 $\pm$ 0.09 $W\,m^{-1}\,K^{-1}$ for a density of 3.33 $\pm$ 0.06 $g\,cm^{-3}$, while Gorham *et al.* reported values from 1.23 to 1.67 $W\,m^{-1}\,K^{-1}$ for densities ranging from 2.67 to 3.12 $g\,cm^{-3}$ (Ref. 28). Our reported averaged value of 1.73 $\pm$ 0.08 $W\,m^{-1}\,K^{-1}$ for a measured density of 2.77 $\pm$ 0.14 $g\,cm^{-3}$ corroborates reasonably well in terms of density to these reported values. This is in agreement with previously established density dependent thermal conductivity models, such as the lower limit for thermal conductivity[39] and the related differential effective medium approximation,[28,46] which serve as reference models to describe the thermal conductivity of amorphous films as a function of their atomic density.

We may notice that, for films with similar densities, our reported value for the thermal conductivity is somewhat higher than other reports, as can be seen from Fig. 8. For measurements on very thin films (<10 nm), ALD-Al_2O_3 films could be inhomogeneous across the film thickness due to the unstable Al:O ratio during the first cycles of the deposition, before reaching a ratio of 2:3 for large cycle numbers.[8] In this scenario, the measurement on

11 August 2023 09:03:29

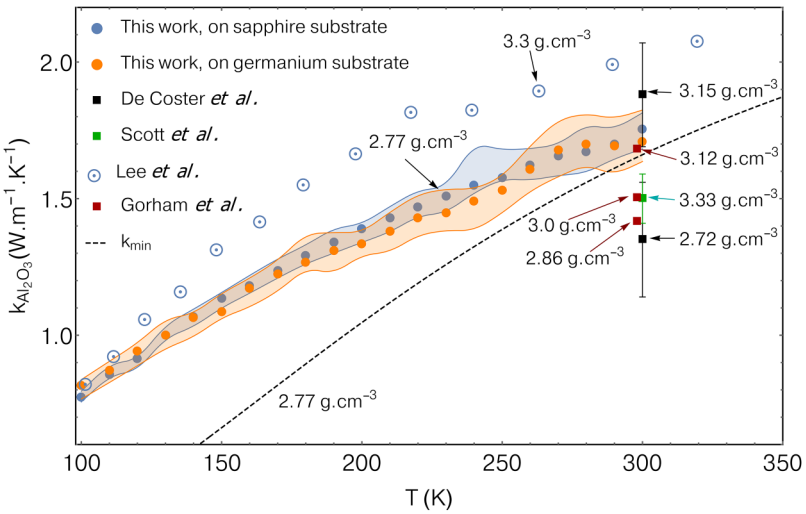

FIG. 8. Temperature dependence of the intrinsic thermal conductivity of ALD-Al_2O_3 thin films deposited on two different substrates. Other data from ALD-Al_2O_3 films with measured density are displayed in comparison, taken from Refs. 21, 28, 29 and 38, while k_{min} is calculated from Ref. 39. Data reported using TDTR are shown as squares, whereas other shapes are from 3ω experiments.

Published under license by AIP Publishing.

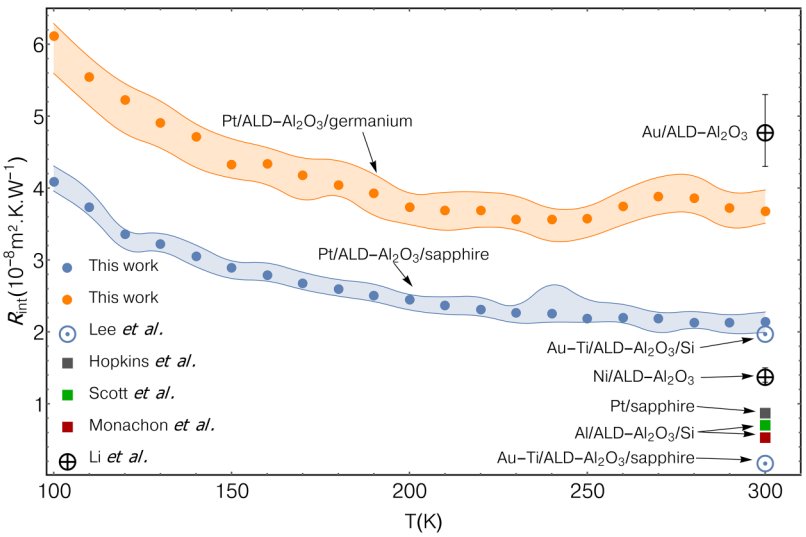

FIG. 9. Temperature dependence of the sum of thermal boundary resistances measured in two different systems, colored bands represent 68% confidence intervals. TBRs from sapphire have lower error bars due to the fact that five thicknesses were used to extract them, as opposed to the four samples used for the germanium substrate. Other TBRs with related materials are taken from Refs. 21, 22, 38, 43 and 63. Data reported using TDTR are shown as squares, whereas other shapes are from 3ω experiments.

very thin films would be more sensitive to inhomogeneity of the films, and could possibly lead to lower thermal conductivity. This could explain the difference between our data and that reported by Scott *et al.*,[38] where the films were between 1 and 10 nm thick with lower thermal conductivity than our films, while having higher density. However, this would not explain our relative difference with data from Gorham *et al.*,[28] since they used films with thicknesses comparable to ours. Thus, additional quantitative structural characterizations of ALD films might prove useful in explaining the relative difference observed in terms of thermal conductivity.

B. Thermal boundary resistances

We see in Fig. 7 the significance of TBRs, weighting up to two third of the measured total thermal resistance, in the case of the thinnest film (17.0 nm) at 300 K grown on sapphire. Even for the thickest film (119.4 nm), the contribution from TBRs weights up to 35% of the total thermal resistance for films deposited on germanium. These considerations support the need to perform multiple measurements on several film thicknesses for accurate thermal characterization when using the 3ω method,[47] even for films having relatively low thermal conductivity. This statement is by all means related to the rather large TBRs measured in this work, when compared to the film thermal resistance.

Figure 9 displays the total TBR measured from Al_2O_3 films deposited on germanium and sapphire. The behavior with temperature is similar for both substrates, and in qualitative agreement with theoretical models predicting an increased TBR between two dissimilar materials as temperature decreases.[48] We clearly observe that the sum of TBRs is larger when the Al_2O_3 film is deposited on germanium compared to the same film deposited on sapphire. Notwithstanding the accurate prediction of TBR is an arduous task in this temperature range,[49] we can still discuss important key experimental points that could warrant the relatively large TBR measured in this work. Indeed, at 300 K, we measure 2.1×10^{-8} and 3.7×10^{-8} m^2 K W^{-1} for TBR extracted from Al_2O_3 films deposited on sapphire and germanium, respectively. These values are comparable with others extracted from 3ω experiments[18,19,21,22,50] but generally lie in the higher end of most TBR reported values.[51] Using a similar 3ω method, Lee *et al.*[21] reported that the sum of TBRs is larger from ALD-Al_2O_3 deposited on silicon ($\approx 2 \times 10^{-8}$ m^2 K W^{-1}) than that deposited on sapphire

11 August 2023 09:03:29

TABLE I. Summary of the measured quantities in this work. $k_{Al_2O_3}$ refers to the intrinsic thermal conductivity of the film, inferred using Eq (2). The substrate thermal conductivity $k_{s,avg}$ is calculated from the mean of the four (five for sapphire) samples measured to deduce the film thermal conductivity. TBR refers to the sum of thermal boundary resistances in series in the system (Pt/Al_2O_3 + Al_2O_3/substrate). Values in brackets are 68% CI.

Substrate	T (K)	$k_{Al_2O_3}$ (W m^{-1} K^{-1})	TBR (10^{-8} m^2 K W^{-1})	$k_{s,avg}$ (W m^{-1} K^{-1})
Germanium	100	0.82 [0.77,0.84]	6.1 [5.6,6.4]	148
	200	1.34 [1.29,1.40]	3.8 [3.5,4.0]	77
	300	1.71 [1.66,1.83]	3.7 [3.6,4.0]	52
Sapphire	100	0.77 [0.76,0.80]	4.1 [4.0,4.3]	335
	200	1.39 [1.34,1.41]	2.5 [2.3,2.5]	65
	300	1.75 [1.68,1.81]	2.1 [2.0,2.3]	34

Published under license by AIP Publishing.

($\approx 2 \times 10^{-9}$ m^2 K W^{-1}), though the amplitude is smaller in their study and they used gold as a transducer using a Ti adhesion layer. The large discrepancy—almost a factor of ten—between the reported value for the Au-Ti/ALD-Al_2O_3/sapphire interface compared to our Pt/ALD-Al_2O_3/sapphire interface suggests that Pt/ALD-Al_2O_3 be the prevalent TBR in this case, as will be discussed later. Besides, in sandwiched structures such as ours containing ALD-Al_2O_3 films, other authors have reported TBRs that are at least two times smaller than our results, using TDTR. Indeed, for Al/Al_2O_3/Si, Monachon and Weber measured $5.2 \pm 0.5 \times 10^{-9}$ m^2 K W^{-1}, while Scott *et al.* reported $6.92 \pm 0.50 \times 10^{-9}$ m^2 K W^{-1}, where the Al layer serving as their opto-thermal transducer, was DC-sputtered or electron-beam evaporated, respectively.[38,43]

The variation between these results and our measurements leads us to discuss two particular points. First, the relative difference between TBRs measured from the sapphire and germanium substrates, and second, the overall large sum of TBRs measured for both substrates. For the first aspect, one possible reason is the presence of a native oxide layer on the substrate, that has not been removed prior to the films deposition. On the germanium substrate, this native oxide could substantially impede thermal transfer across the interface, hence increasing the measured TBR.[52] It has been shown in Refs. 8 and 53 that, even after removing the native oxide from the germanium substrate prior to ALD, a germanium oxide would eventually re-form at the interface during the deposition process, with thickness ≈0.2–0.5 nm. This would partly explain the difference observed between both substrates, in addition to the greater contrast that exists in terms of mass density and speed of sound between the germanium/ALD-Al_2O_3 interface compared to the sapphire/ALD-Al_2O_3 interface. This would lead to a higher TBR for the germanium/ALD-Al_2O_3 interface, as predicted by the Diffuse Mismatch Model (DMM).[48,54,55]

To have an estimation of how the contrast in thermal properties between two materials might lead to significant change on their thermal boundary resistance, we use a gray approximation of the DMM[56] and estimate the thermal boundary resistance as $\mathrm{TBR} = \left(\frac{C_i v_i}{4}\frac{C_j v_j}{C_i v_i + C_j v_j}\right)^{-1}$, where C_i and v_i stand for the volumetric heat capacity (in J m^{-3} K^{-1}) and phonon group velocity (in m s^{-1}) of material i, respectively—an approach that have been used in Ref. 38. For the ALD-Al_2O_3 films and sapphire substrate, we assume $v = 8800$ m s^{-1} for their longitudinal speed of sound,[57] while for the germanium substrate we use $v = 6240$ m s^{-1}(Ref. 58). For the volumetric heat capacity, we use our measured value of the heat capacity for the sapphire and germanium substrates combined with the mass density taken from the literature.[59] For the ALD-Al_2O_3 films, we use the measured heat capacity of the sapphire substrate combined with the film density that has been measured using RBS. These lead to the volumetric heat capacity of $C_{\mathrm{sapphire}} = 3.05$ MJ m^{-3} K^{-1}, $C_{\mathrm{germanium}} = 1.72$ MJ m^{-3} K^{-1} and $C_{\mathrm{ALD-Al_2O_3}} = 2.15$ MJ m^{-3} K^{-1}. Using the aforementioned thermal and structural properties, we arrive at $\mathrm{TBR}_{\mathrm{ALD-Al_2O_3/germanium}} = 1.6 \times \mathrm{TBR}_{\mathrm{ALD-Al_2O_3/sapphire}}$, which is in reasonable agreement with what is observed experimentally in this work. Using GeO_2 instead of Ge, with volumetric heat capacity and longitudinal speed of sound taken from Ref. 27, we obtain $\mathrm{TBR}_{\mathrm{ALD-Al_2O_3/GeO_2}} \approx 3 \times \mathrm{TBR}_{\mathrm{ALD-Al_2O_3/sapphire}}$. We emphasize that this calculation is only qualitative but agrees relatively well with the trend that is observed here. Thus, the higher TBRs for the germanium substrate can be understood using the aforementioned arguments.

For the second aspect—the relatively high TBR measured for both substrates—we remind that the platinum transducer was DC-sputtered without any adhesion layer. A recent work from Suk and Kim[60] suggests that DC magnetron sputtered films have more imperfections at the film/substrate interface—when compared to other metal deposition techniques such as e-gun evaporation—due to its energetic deposition process, hence increasing the TBR. Most importantly, the use of a metallic adhesion layer is reported to enhance thermal interfacial conductance. Indeed, Li *et al.*[22] have reported a 70% reduction of the TBR between amorphous ALD-Al_2O_3 and gold after introducing a nickel layer, thereby reducing it from 4.8×10^{-8} m^2 K W^{-1} to 1.4×10^{-8} m^2 K W^{-1}, while Jeong *et al.* succeeded in reducing metal/sapphire TBR by a factor from 2 to 4 by inserting a thin metallic adhesion layer,[61] a result reproduced by Blank and Weber.[62] These arguments go in favor of a higher TBR for DC-sputtered films, in particular, when no adhesion layer is used.

Hopkins *et al.* reported TBR of 8.6×10^{-9} m^2 K W^{-1} for a Pt/sapphire interface using TDTR.[63] We can reasonably take this value to serve as a lower bound for our Pt/ALD-Al_2O_3 interface, since the contrast in density is higher in the case of Pt/ALD-Al_2O_3 than for the Pt/sapphire interface—all other parameters assumed to remain constant. Therefore, the thermal contribution of the Pt/ALD-Al_2O_3 TBR would account for *at least* 40% of the total Pt/ALD-Al_2O_3/sapphire TBR, while for the germanium substrate, its contribution would be 23%. While further experiments using other metals as transducers or using a metallic adhesion layer would help to give further insight into the contribution of each interface to the total resistance measured, altogether, the arguments presented above qualitatively justify our findings in terms of relative amplitude of the measured TBRs for both substrates.

11 August 2023 09:03:29

IV. CONCLUSION

In this work, we have measured the thermal conductivity of Al_2O_3 thin films ranging from 17 to 119 nm in thickness that were deposited using Atomic Layer Deposition on sapphire and germanium substrates. The 3ω method has been used, and the data reduction procedure along with the uncertainty analysis was described. The reported value of the thin films' thermal conductivity is found to be in very good agreement with what has been reported so far in the literature. A comparison of the films thermal conductivity in terms of their mass density further emphasizes on the importance of this parameter for achieving optimal thermal performances, an important concern in designing efficient micro-scaled devices. In addition, TBR of the system Pt/Al_2O_3/substrate is shown to be heavily substrate-dependent, with almost a factor of 2 higher for the germanium substrate, in comparison to the sapphire one—a behavior that is justified qualitatively using a DMM approach. If further measurements using other metals as transducers and/or using an adhesion layer would prove useful in separating the contribution from the heater/film TBR to that of the film/substrate, these results provide additional insights into the impact of interfaces in the case of ALD-Al_2O_3 on semiconducting or dielectric materials, in

Published under license by AIP Publishing.

particular, for germanium. Additionally, our results suggest that particular attention should be given to the Pt/ALD-Al_2O_3 interface in electro-thermal measurement, which can represent a substantial fraction of the overall measured thermal resistance.

ACKNOWLEDGMENTS

The authors would like to acknowledge the technical support provided by Institut Néel, the Pole Capteur, especially E. André and G. Moiroux for the platinum deposition, Nanofab for clean room process, and E. Mossang and O. Leynaud from the Pole X'Press for XRR measurements. The authors are grateful to C. Marrache and C. Bachelet for the RBS measurements. The authors also thank K. Termentzidis and D. Lacroix for discussions. This work was supported by the Agence Nationale de la Recherche by the MESOPHON (Project Grant No. ANR-15-CE30-0019) and the Laboratoire d'excellence LANEF in Grenoble (No. ANR-10-LABX-51-01).

APPENDIX: THERMAL MODELLING AND SENSITIVITY IN 3ω EXPERIMENTS

1. Validity of the thermal model for data reduction

We discuss under which conditions the model we use to fit the temperature oscillation [Eq. (1)] is valid. In particular, we discuss the assumption that the experiment is only sensitive to the sum of TBRs and that the film heat capacity does not play a role in the present configuration, leading to model the film as a thermal resistance in series with the heater/thermometer.

The expression of the temperature oscillation amplitude for a film-on-substrate system in a 3ω geometry, including thermal boundary resistances, is derived by solving the 2D heat equation using Fourier Transforms and subsequent spatial averaging over the transducer width. The only difference with the solution provided in Ref. 25 is the inclusion of the film/substrate TBR, $R_{f/s}$. It leads to

$$\Delta T_{2\omega} = \frac{p}{2\pi l}\int_{-\infty}^{\infty} \frac{\sin^2(\lambda b)}{(\lambda b)^2}\frac{1}{k_f\gamma_f \tanh(\gamma_f d_f)}\frac{\left(1+\tanh(\gamma_s d_s)\gamma_s k_s\left(R_{f/s}+\frac{\tanh(\gamma_f d_f)}{k_f\gamma_f}\right)\right)}{\left(1+\tanh(\gamma_s d_s)\gamma_s k_s\left(R_{f/s}+\frac{\coth(\gamma_f d_f)}{k_f\gamma_f}\right)\right)}d\lambda + \frac{p}{2bl}R_{h/f}, \tag{A1a}$$

$$\gamma_i = \sqrt{k_{xy,i}\lambda^2 + i2\omega_e\frac{\rho_i C_{p_i}}{k_i}}. \tag{A1b}$$

To compare this expression to the one we use in the main text, we provide a sensitivity analysis of Eq. (A1). The sensitivity of ΔT to parameter p is defined as[64]

$$S_p^{\Delta T} = \frac{p}{\Delta T}\frac{\partial(\Delta T)}{\partial p} = \frac{\partial(\ln(\Delta T))}{\partial(\ln(p))} \tag{A2}$$

and thus reflects the relative change of ΔT that is induced by a relative change of p. The absolute value of the sensitivity to the Temperature Oscillation (TO) is plotted in Fig. 10(a) for the heater/film interface $R_{h/f}$, film/substrate interface $R_{f/s}$, and film heat capacity $(\rho Cp)_{Al_2O_3}$. As is expected from the frequency range that is spanned during these 3ω experiments, we cannot discriminate $R_{h/f}$ from $R_{f/s}$ since the thermal penetration depth is always much larger than the film thickness. This is reflected on the sensitivity plots, which have similar frequency dependence for both TBRs. For the thickest (119 nm) film, distinguishing the contribution of $R_{h/f}$ to that of $R_{f/s}$ would require to increase the frequency up to a few MHz, which is not possible using our current setup and is better suited to optical experiments. Therefore, in our experiments, we are always sensitive to the quantity $(R_{h/f}+R_{f/s}) = R_{int}$, since in the present configuration, there is no other parameter to play with that would increase the sensitivity of only one of the two TBRs. This is further emphasized in Fig. 10(b), where we plot Eq. (A1) using two different pairs of $\{R_{h/f},R_{f/s}\}$, keeping $(R_{h/f}+R_{f/s})$ constant. In comparison, we plot Eq. (1) using the same value of $(R_{h/f}+R_{f/s})$. The three plots overlap, confirming the assumption that we are only sensitive to the sum of both TBRs.

The sensitivity of the TO to the film heat capacity is almost null on the entire frequency range spanned during the experiment, suggesting that Eqs. (1) and (2) are indeed a very good approximation to Eq. (A1) [which can be seen as well in Fig. 10(b)]. Therefore, given the film thickness and the frequency range spanned during the experiment, the film can be simply modeled as a thermal resistance in series with the heater/thermometer, and thus only adds a frequency independent offset to the temperature oscillation, as detailed in Ref. 25. These arguments make valid the use of Eqs. (1) and (2).

2. Sensitivity of the temperature oscillation to k_i and R_{int}

The sensitivity of the TO [Eq. (1)] to the film intrinsic thermal conductivity k_i (solid lines) and R_{int} (dashed lines) is plotted in Figs. 10(c) and 10(d) for both substrates using values extracted at 300 K. These results suggest that, given the amplitude of R_{int}, it is mandatory to use several thicknesses of the film to accurately extract the film intrinsic thermal conductivity. Indeed, the sensitivity to R_{int} is, for the thinnest film and for both substrates, higher than the sensitivity to k_i. For thicker films, the sensitivity to R_{int} decreases but still remains significant.

3. Error coming from the substrate's thermal anisotropy

We made the assumption $k_{s_{xy}} = 1.1$ for the sapphire substrate when fitting our measured data to Eq. (1). While the consequence of this assumption is taken into account while performing the

11 August 2023 09:03:29

Published under license by AIP Publishing.

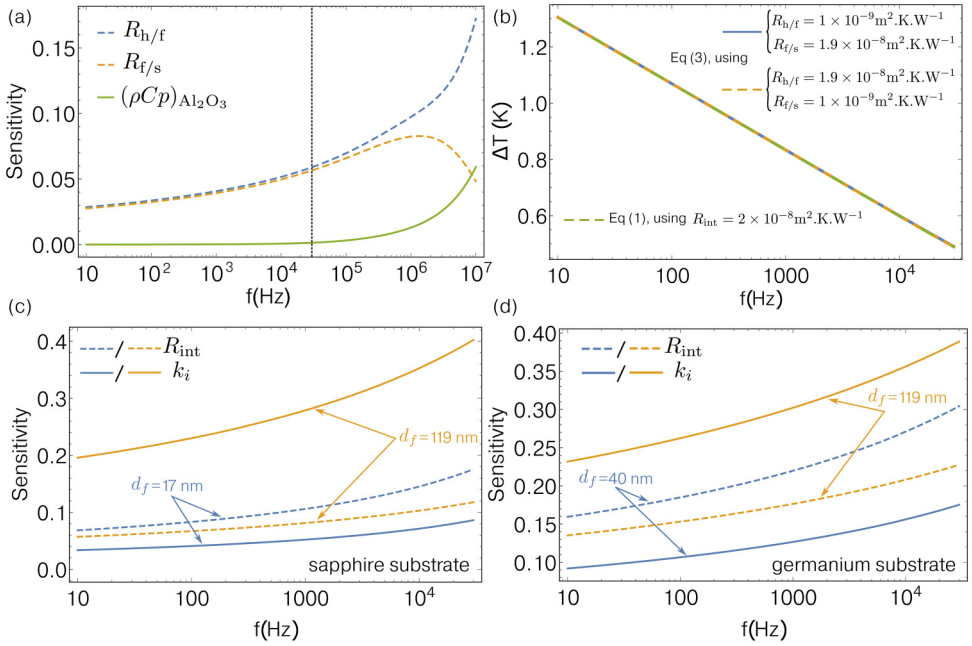

FIG. 10. (a) Sensitivity of the temperature oscillation to the heater/film interface $R_{h/f}$, film/substrate interface $R_{f/s}$ and film heat capacity $(\rho Cp)_{Al_2O_3}$ for a 119 nm film on a sapphire substrate at 300 K. (b) Several combinations of the quantity $R_{h/f}$+$R_{f/s}$ using Eq. (A1) lead to the same measured temperature oscillation that is obtained using Eq. (1), emphasizing that we are only sensitive to the quantity $R_{int} = R_{h/f}$+$R_{f/s}$. (c) and (d) Absolute value of the sensitivity of the temperature oscillation to R_{int} and k_i, for both substrates.

11 August 2023 09:03:29

uncertainty analysis, where the anisotropy is changed from 1 to 1.3, we discuss quantitatively how this parameter impact the extracted thermal parameter when using the 3ω method, since it is not straightforward when simply looking to the error bars provided by the uncertainty analysis. We consider the case where one would assume $k_{s_{xy}} = 1$ for the fitting, while the substrate has in fact anisotropic thermal properties. This assumption $k_{s_{xy}} = 1$ would lead to two consequences. First, it would result in measuring the "average" substrate's thermal conductivity $k_s = \sqrt{k_{s_x} k_{s_y}}$, which is the quantity that is always measured in a 3ω experiment when using the "slope method."[25,65] Second, and most importantly, it would add a frequency independent offset to R_{th}, with magnitude $\frac{b}{2\pi}\frac{\ln(k_{s_{xy}})}{\sqrt{k_{s_x} k_{s_y}}}$. This contribution can be derived by writing Eq. (1) in the limit where $|1/q| > b$ and rearranging. In the limit $|1/q| > b$, Eq (1) can, therefore, be rewritten as

$$\Delta T_{2\omega} = \frac{p}{\pi l k_{s_y}} \int_0^\infty \frac{1}{\sqrt{k_{s_{xy}}\lambda^2 + \frac{i2\omega_e \rho_s C_{ps}}{k_{s_y}}}\tanh\left(\sqrt{k_{s_{xy}}\lambda^2 + \frac{i2\omega_e \rho_s C_{ps}}{k_{s_y}}} d_s\right)} \frac{\sin^2(b\lambda)}{(b\lambda)^2} d\lambda + \frac{p}{2bl} R_{th}$$
$$\approx \frac{p}{\pi l \sqrt{k_{s_x} k_{s_y}}} \int_0^\infty \frac{1}{\sqrt{\lambda^2 + \frac{i2\omega_e \rho_s C_{ps}}{\sqrt{k_{s_x} k_{s_y}}}}\tanh\left(\sqrt{\lambda^2 + \frac{i2\omega_e \rho_s C_{ps}}{\sqrt{k_{s_x} k_{s_y}}}} d_s\right)} \frac{\sin^2(b\lambda)}{(b\lambda)^2} d\lambda + \frac{p}{2bl}\left(R_{th} + \frac{b}{2\pi}\frac{\ln(k_{s_{xy}})}{\sqrt{k_{s_x} k_{s_y}}}\right). \quad \text{(A3)}$$

While measuring the thermal conductivity of the substrate is not of prime importance in this study, the thermal conductivity of the films and TBRs depends upon the quantity R_{th}, as explained in the main text. From Eq. (A3), the absolute error on R_{th} is equal to $\frac{b}{2\pi}\frac{\ln(k_{s_{xy}})}{\sqrt{k_{s_x} k_{s_y}}}$. Therefore, if the true substrate anisotropy is $k_{s_{xy}} \approx 1.1 - 1.3$, the resulting error on R_{th} would be $\approx 1.1 - 3.0 \times 10^{-9}$ m² K W⁻¹ for the sapphire substrate at 300 K and decrease at lower temperatures due to the increase of the substrate's thermal conductivity. These conservative estimates on $k_{s_{xy}}$ are based upon separate 2ω experiments performed using the

Published under license by AIP Publishing.

method proposed in Ref. 66. While an accurate measurement of $k_{s_{xy}}$ is a difficult task given the small anisotropy of the substrate, we always obtained $k_{s_{xy}} > 1$, meaning that R_{int} can only be somewhat overestimated, not underestimated. In any cases, the film's thermal conductivity k_i remains unaffected since its value depends on the slope of $R_{\text{th}} = \text{f}(d_f)$, while the error is a constant offset.

DATA AVAILABILITY

The data that support the findings of this study are available from the corresponding authors upon reasonable request.

REFERENCES

[1]Z. Hu, K. Nomoto, W. Li, N. Tanen, K. Sasaki, A. Kuramata, T. Nakamura, D. Jena, and H. G. Xing, "Enhancement-mode Ga_2O_3 vertical transistors with breakdown voltage >1 kV," IEEE Electron Device Lett. **39**, 869–872 (2018).

[2]Y. Hsu, X. Fang, L. A. Wang, H.-W. Zan, H.-F. Meng, and S.-H. Yang, "Sub-100 nm ALD-assisted nanoimprint lithography for realizing vertical organic transistors with high ON/OFF ratio and high output current," Org. Electron. **15**, 3609–3614 (2014).

[3]M. J. Biercuk, D. J. Monsma, C. M. Marcus, J. S. Becker, and R. G. Gordon, "Low-temperature atomic-layer-deposition lift-off method for microelectronic and nanoelectronic applications," Appl. Phys. Lett. **83**, 2405–2407 (2003).

[4]M. D. Groner, F. H. Fabreguette, J. W. Elam, and S. M. George, "Low-temperature Al_2O_3 atomic layer deposition," Chem. Mater. **16**, 639–645 (2004).

[5]S. M. George, "Atomic layer deposition: An overview," Chem. Rev. **110**, 111–131 (2010).

[6]A. Toriumi, T. Tabata, C. Hyun Lee, T. Nishimura, K. Kita, and K. Nagashio, "Opportunities and challenges for Ge CMOS—Control of interfacing field on Ge is a key (invited paper)," Microelectron. Eng. **86**, 1571–1576 (2009).

[7]R. Pillarisetty, "Academic and industry research progress in germanium nanodevices," Nature **479**, 324–328 (2011).

[8]S. Swaminathan, Y. Sun, P. Pianetta, and P. C. McIntyre, "Ultrathin ALD-Al_2O_3 layers for Ge(001) gate stacks: Local composition evolution and dielectric properties," J. Appl. Phys. **110**, 094105 (2011).

[9]K. El hajraoui, M. A. Luong, E. Robin, F. Brunbauer, C. Zeiner, A. Lugstein, P. Gentile, J.-L. Rouvière, and M. Den Hertog, "In situ transmission electron microscopy analysis of aluminum–germanium nanowire solid-state reaction," Nano Lett. **19**, 2897–2904 (2019).

[10]D. Singhal, J. Paterson, M. Ben-Khedim, D. Tainoff, L. Cagnon, J. Richard, E. Chavez-Angel, J. J. Fernandez, C. M. Sotomayor-Torres, D. Lacroix, D. Bourgault, D. Buttard, and O. Bourgeois, "Nanowire forest of pnictogen–chalcogenide alloys for thermoelectricity," Nanoscale **11**, 13423–13430 (2019).

[11]D. Singhal, J. Paterson, D. Tainoff, J. Richard, M. Ben-Khedim, P. Gentile, L. Cagnon, D. Bourgault, D. Buttard, and O. Bourgeois, "Measurement of anisotropic thermal conductivity of a dense forest of nanowires using the 3 ω method," Rev. Sci. Instrum. **89**, 084902 (2018), arXiv:1811.08732

[12]S. D. Lubner, S. Kaur, Y. Fu, V. Battaglia, and R. S. Prasher, "Identification and characterization of the dominant thermal resistance in lithium-ion batteries using operando 3-omega sensors," J. Appl. Phys. **127**, 105104 (2020).

[13]A. J. Minnich, J. A. Johnson, A. J. Schmidt, K. Esfarjani, M. S. Dresselhaus, K. A. Nelson, and G. Chen, "Thermal conductivity spectroscopy technique to measure phonon mean free paths," Phys. Rev. Lett. **107**, 095901 (2011).

[14]L. Zeng, K. C. Collins, Y. Hu, M. N. Luckyanova, A. A. Maznev, S. Huberman, V. Chiloyan, J. Zhou, X. Huang, K. A. Nelson, and G. Chen, "Measuring phonon mean free path distributions by probing quasiballistic phonon transport in grating nanostructures," Sci. Rep. **5**, 17131 (2015).

[15]A. T. Ramu, N. I. Halaszynski, J. D. Peters, C. D. Meinhart, and J. E. Bowers, "An electrical probe of the phonon mean-free path spectrum," Sci. Rep. **6**, 33571 (2016).

[16]A. Tavakoli, K. Lulla, T. Crozes, N. Mingo, E. Collin, and O. Bourgeois, "Heat conduction measurements in ballistic 1D phonon waveguides indicate breakdown of the thermal conductance quantization," Nat. Commun. **9**, 4287 (2018).

[17]D. G. Cahill, "Thermal conductivity measurement from 30 to 750 K: The 3ω method," Rev. Sci. Instrum. **61**, 802–808 (1990).

[18]J. H. Kim, A. Feldman, and D. Novotny, "Application of the three omega thermal conductivity measurement method to a film on a substrate of finite thickness," J. Appl. Phys. **86**, 3959–3963 (1999).

[19]T. Yamane, N. Nagai, S.-I. Katayama, and M. Todoki, "Measurement of thermal conductivity of silicon dioxide thin films using a 3ω method," J. Appl. Phys. **91**, 9772 (2002).

[20]W. Jang, Z. Chen, W. Bao, C. N. Lau, and C. Dames, "Thickness-dependent thermal conductivity of encased graphene and ultrathin graphite," Nano Lett. **10**, 3909–3913 (2010).

[21]S.-M. Lee, W. Choi, J. Kim, T. Kim, J. Lee, S. Y. Im, J. Y. Kwon, S. Seo, M. Shin, and S. E. Moon, "thermal conductivity and thermal boundary resistances of ALD Al_2O_3 films on Si and sapphire," Int. J. Thermophys. **38**, 176 (2017).

[22]X. Li, W. Park, Y. Wang, Y. P. Chen, and X. Ruan, "Reducing interfacial thermal resistance between metal and dielectric materials by a metal interlayer," J. Appl. Phys. **125**, 045302 (2019).

[23]D. G. Cahill, "Erratum: 'Thermal conductivity measurement from 30 to 750 K: The 3ω method' [Rev. Sci. Instrum. 61, 802 (1990)]," Rev. Sci. Instrum. **73**, 3701–3701 (2002).

[24]A. T. Ramu and J. E. Bowers, "Analysis of the '3-omega' method for substrates and thick films of anisotropic thermal conductivity," J. Appl. Phys. **112**, 043516 (2012).

[25]T. Borca-Tasciuc, A. R. Kumar, and G. Chen, "Data reduction in 3ω method for thin-film thermal conductivity determination," Rev. Sci. Instrum. **72**, 2139–2147 (2001).

[26]S.-M. Lee and D. G. Cahill, "Heat transport in thin dielectric films," J. Appl. Phys. **81**, 2590–2595 (1997).

[27]R. O. Pohl, X. Liu, and E. Thompson, "Low-temperature thermal conductivity and acoustic attenuation in amorphous solids," Rev. Mod. Phys. **74**, 991–1013 (2002).

[28]C. S. Gorham, J. T. Gaskins, G. N. Parsons, M. D. Losego, and P. E. Hopkins, "Density dependence of the room temperature thermal conductivity of atomic layer deposition-grown amorphous alumina (Al_2O_3)," Appl. Phys. Lett. **104**, 253107 (2014).

[29]M. E. DeCoster, K. E. Meyer, B. D. Piercy, J. T. Gaskins, B. F. Donovan, A. Giri, N. A. Strnad, D. M. Potrepka, A. A. Wilson, M. D. Losego, and P. E. Hopkins, "Density and size effects on the thermal conductivity of atomic layer deposited TiO_2 and Al_2O_3 thin films," Thin Solid Films **650**, 71–77 (2018).

[30]P. A. Premkumar, A. Delabie, L. N. J. Rodriguez, A. Moussa, and C. Adelmann, "Roughness evolution during the atomic layer deposition of metal oxides," J. Vac. Sci. Technol. A **31**, 061501 (2013).

[31]Change in the stoichiometric composition of the films, which could potentially lead to dissimilar surfaces for films of increasing thicknesses, is reported to appear during the first cycles (≈60) of the deposition process.[8] Since the present films are least 17 nm thick (145 cycles), we suppose that the films top surfaces do not exhibit large structural and stoichiometric changes as a function of their thickness.

[32]A. Saltelli, M. Ratto, T. Andres, F. Campolongo, J. Cariboni, D. Gatelli, M. Saisana, and S. Tarantola, *Global Sensitivity Analysis. The Primer* (John Wiley and Sons, Ltd, Chichester, UK, 2008), pp. 1–292

[33]Z. Chen and C. Dames, *Applied Thermal Measurements at the Nanoscale*, Lessons from Nanoscience: A Lecture Notes Series, Vol. 7 (World Scientific, 2018).

[34]D. G. Cahill, S.-M. Lee, and T. I. Selinder, "Thermal conductivity of κ-Al_2O_3 and α-Al_2O_3 wear-resistant coatings," J. Appl. Phys. **83**, 5783–5786 (1998).

[35]M. Rahman, M. Shahzadeh, and S. Pisana, "Simultaneous measurement of anisotropic thermal conductivity and thermal boundary conductance of 2-dimensional materials," J. Appl. Phys. **126**, 205103 (2019).

11 August 2023 09:03:29

Published under license by AIP Publishing.

[36]J. A. Carruthers, T. H. Geballe, H. M. Rosenberg, and J. M. Ziman, "The thermal conductivity of germanium and silicon between 2 and 300 K," Proc. R. Soc. Lond. A **238**, 502–514 (1957).
[37]C. J. Glassbrenner and G. A. Slack, "Thermal conductivity of silicon and germanium from 3 K to the melting point," Phys. Rev. **134**, A1058–A1069 (1964).
[38]E. A. Scott, J. T. Gaskins, S. W. King, and P. E. Hopkins, "Thermal conductivity and thermal boundary resistance of atomic layer deposited high-k dielectric aluminum oxide, hafnium oxide, and titanium oxide thin films on silicon," APL Mater. **6**, 058302 (2018).
[39]D. G. Cahill, S. K. Watson, and R. O. Pohl, "Lower limit to the thermal conductivity of disordered crystals," Phys. Rev. B **46**, 6131–6140 (1992).
[40]I. Stark, M. Stordeur, and F. Syrowatka, "Thermal conductivity of thin amorphous alumina films," Thin Solid Films **226**, 185–190 (1993).
[41]S.-M. Lee, D. G. Cahill, and T. H. Allen, "Thermal conductivity of sputtered oxide films," Phys. Rev. B **52**, 253–257 (1995).
[42]A. Cappella, J.-L. Battaglia, V. Schick, A. Kusiak, A. Lamperti, C. Wiemer, and B. Hay, "High temperature thermal conductivity of amorphous Al_2O_3 thin films grown by low temperature ALD," Adv. Eng. Mater. **15**, 1046–1050 (2013).
[43]C. Monachon and L. Weber, "Influence of a nanometric Al_2O_3 interlayer on the thermal conductance of an Al/(Si, diamond) interface," Adv. Eng. Mater. **17**, 68–75 (2015).
[44]Z. Luo, H. Liu, B. T. Spann, Y. Feng, P. Ye, Y. P. Chen, and X. Xu, "Measurement of in-plane thermal conductivity of ultrathin films using micro-raman spectroscopy," Nanoscale Microscale Thermophys. Eng. **18**, 183–193 (2014).
[45]Atomic densities of 8.02×10^{28} and 9.29×10^{28} atoms m^{-3} were converted in units of g cm^{-3} assuming a Al:O ratio of 2:3.
[46]R. M. Costescu, A. J. Bullen, G. Matamis, K. E. O'Hara, and D. G. Cahill, "Thermal conductivity and sound velocities of hydrogen-silsesquioxane low-*k* dielectrics," Phys. Rev. B **65**, 094205 (2002).
[47]T. Tong and A. Majumdar, "Reexamining the 3-omega technique for thin film thermal characterization," Rev. Sci. Instrum. **77**, 104902 (2006).
[48]E. T. Swartz and R. O. Pohl, "Thermal boundary resistance," Rev. Mod. Phys. **61**, 605–668 (1989).
[49]C. Monachon, L. Weber, and C. Dames, "Thermal boundary conductance: A materials science perspective," Annu. Rev. Mater. Res. **46**, 433–463 (2016).
[50]X. Li, Y. Yan, L. Dong, J. Guo, A. Aiyiti, X. Xu, and B. Li, "Thermal conduction across a boron nitride and SiO_2 interface," J. Phys. D Appl. Phys. **50**, 104002 (2017).
[51]A. Giri and P. E. Hopkins, "A review of experimental and computational advances in thermal boundary conductance and nanoscale thermal transport across solid interfaces," Adv. Funct. Mater. **30**, 1903857 (2019).
[52]C. Monachon, M. Hojeij, and L. Weber, "Influence of sample processing parameters on thermal boundary conductance value in an Al/AlN system," Appl. Phys. Lett. **98**, 091905 (2011).
[53]M. Botzakaki, A. Kerasidou, L. Sygellou, V. Ioannou-Sougleridis, N. Xanthopoulos, S. Kennou, S. Ladas, N. Z. Vouroutzis, T. Speliotis, and D. Skarlatos, "Interfacial properties of ALD-deposited Al_2O_3/p-type germanium MOS structures: Influence of oxidized Ge interfacial layer dependent on Al_2O_3 thickness," ECS Solid State Lett. **1**, P32–P34 (2012).
[54]S. Merabia and K. Termentzidis, "Thermal conductance at the interface between crystals using equilibrium and nonequilibrium molecular dynamics," Phys. Rev. B **86**, 094303 (2012).
[55]A. France-Lanord, S. Merabia, T. Albaret, D. Lacroix, and K. Termentzidis, "Thermal properties of amorphous/crystalline silicon superlattices," J. Phys. Condens. Matter **26**, 355801 (2014).
[56]G. Chen, "Thermal conductivity and ballistic-phonon transport in the cross-plane direction of superlattices," Phys. Rev. B **57**, 14958–14973 (1998).
[57]C. T. Lynch, *Practical Handbook of Materials Science*, 1st ed. (CRC Press, 1989).
[58]M. D. Tiwari and B. K. Agrawal, "Analysis of the lattice thermal conductivity of germanium," Phys. Rev. B **4**, 3527–3532 (1971).
[59]J. F. Shackelford, Y.-H. Han, S. Kim, and S.-H. Kwon, *CRC Materials Science and Engineering Handbook* (CRC Press, 2016).
[60]M. E. Suk and Y. Y. Kim, "Influence of deposition techniques on the thermal boundary resistance of aluminum thin-films," Int. J. Precis. Eng. Manuf. **20**, 1435–1441 (2019).
[61]M. Jeong, J. P. Freedman, H. J. Liang, C.-M. Chow, V. M. Sokalski, J. A. Bain, and J. A. Malen, "Enhancement of thermal conductance at metal-dielectric interfaces using subnanometer metal adhesion layers," Phys. Rev. Appl. **5**, 014009 (2016).
[62]M. Blank and L. Weber, "Influence of the thickness of a nanometric copper interlayer on Au/dielectric thermal boundary conductance," J. Appl. Phys. **124**, 105304 (2018).
[63]P. E. Hopkins, R. N. Salaway, R. J. Stevens, and P. M. Norris, "Temperature-dependent thermal boundary conductance at Al/Al_2O_3 and Pt/Al_2O_3 interfaces," Int. J. Thermophys. **28**, 947–957 (2007).
[64]D. M. Hamby, "A review of techniques for parameter sensitivity," Environ. Monit. Assess. **32**, 135–154 (1994).
[65]V. Mishra, C. L. Hardin, J. E. Garay, and C. Dames, "A 3 omega method to measure an arbitrary anisotropic thermal conductivity tensor," Rev. Sci. Instrum. **86**, 054902 (2015).
[66]A. T. Ramu and J. E. Bowers, "A "2-omega" technique for measuring anisotropy of thermal conductivity," Rev. Sci. Instrum. **83**, 124903 (2012).

11 August 2023 09:03:29

Published under license by AIP Publishing.